

# Theory of electromagnon in the multiferroic Mn perovskites — Vital role of higher harmonic components of the spiral spin order —

Masahito Mochizuki,<sup>1,\*</sup> Nobuo Furukawa,<sup>2,3,†</sup> and Naoto Nagaosa<sup>1,4,‡</sup>

<sup>1</sup>*Department of Applied Physics, The University of Tokyo,  
7-3-1, Hongo, Bunkyo-ku, Tokyo 113-8656, Japan*

<sup>2</sup>*Department of Physics, Aoyama Gakuin University, Fuchinobe 5-10-1, Sagami-hara, 229-8558 Japan*

<sup>3</sup>*Multiferroics Project, ERATO, Japan Science and Technology Agency (JST) c/o Department of Applied Physics,  
The University of Tokyo, Tokyo 113-8656, Japan*

<sup>4</sup>*Cross-Correlated Materials Research Group, RIKEN, Saitama 351-0198, Japan*

We study theoretically the electromagnon and its optical spectrum (OS) of the terahertz-frequency regime in the magnetic-spiral-induced multiferroic phases of the rare-earth (*R*) Mn perovskites,  $RMnO_3$ , taking into account the elliptical deformation or the higher harmonics of the spiral spin configuration, which has been missed so far. A realistic spin Hamiltonian, which gives phase diagrams in agreement with experiments, resolves a long standing puzzle, i.e., the double-peak structure of the OS with a larger low-energy peak originating from magnon modes hybridized with the zone-edge state. We also predict the magnon branches associated with the electromagnon, which can be tested by neutron-scattering experiment.

PACS numbers: 75.80.+q, 75.40.Gb, 75.30.Ds, 76.50.+g

The charge dynamics below the Mott gap in Mott insulators is an issue of intensive recent interest. The rich structures of the low-energy optical spectrum (OS) are associated with the spin degree of freedom in so-called multiferroics, which shows both magnetic order and ferroelectricity [1]. The spontaneous electric polarization in these materials is driven by the magnetic ordering, and the strong coupling between the dynamics of electric polarization and magnetism is inevitable. In particular, in the rare-earth (*R*) perovskite manganites  $RMnO_3$  [2], which is the main target of this paper, the relativistic spin-orbit interaction and the spin current play essential roles in the multiferroic behavior [3–5]. Excitations of the magnet are usually described as the spin wave or the magnon, i.e., a harmonic oscillation of spins around their ground-state configuration. It couples to the electric polarization in the multiferroics, and thus is termed electromagnon [6]. It is crucial to understand the OS of the electromagnon to design the giant magnetoelectric coupling in the terahertz-frequency regime.

In  $RMnO_3$ , frustration between the spin-exchange interactions leads to a non-collinear spin spiral in the ground state. This simple idea, however, cannot explain the rich phase diagrams in the plane of Mn-O-Mn bond angle and temperature, and also those under magnetic fields. In real systems, there are other interactions originating from the relativistic spin-orbit interaction such as the magnetic anisotropy and the Dzyaloshinskii-Moriya (DM) interaction. By studying a realistic spin Hamiltonian taking into account these interactions, the phase diagrams including the spin-flop transition have been understood except for the collinear E-type spin phase [7]. It turned out that coupling of the spins to phonons given by  $\mathcal{H}_{sp} = \sum_{ij} gQ_{ij}\tilde{S}_i \cdot \tilde{S}_j$  plays an important role to stabilize the E-type phase, which is expected to play some

roles even in the neighboring spiral phases.

On the other hand, after the first experimental observation of the terahertz OS in the multiferroic  $RMnO_3$  [8, 9], it was interpreted as a collective mode corresponding to rotation of the spin-spiral plane associated with fluctuations of the polarization direction [10]. Later it turned out that the selection rule and the magnitude of oscillator strength ruled out this interpretation [11, 12], and a new mechanism has been searched for. The most promising candidate is the conventional magnetostriction mechanism [13, 14], where the electric polarization  $\mathbf{P}$  is given by

$$\mathbf{P} = \sum_{ij} \mathbf{\Pi}_{ij} (\mathbf{S}_i \cdot \mathbf{S}_j). \quad (1)$$

Here the vector  $\mathbf{\Pi}_{ij}$  is nonzero in  $RMnO_3$  since the inversion symmetry is absent at the center of the Mn-O-Mn bond because of the orthorhombic lattice distortion and/or the staggered  $d_{3x^2-r^2}/d_{3y^2-r^2}$  orbital ordering. This contribution cancels out in the ground state due to the symmetry, but the dynamical fluctuations of  $\mathbf{P}$  contribute to the electromagnon excitation. Especially, in the non-collinear ground state, the single magnon processes at the zone edge originate from Eq. (1). However, this scenario cannot explain the low-energy peak at  $\sim 2$ -3 meV (see insets of Fig. 2), which is comparable to or even larger than the high-energy peak at  $\sim 5$ -8 meV in  $DyMnO_3$  [11],  $TbMnO_3$  [15], and  $Eu_{1-x}Y_xMnO_3$  [16]. Therefore, the puzzle still remains.

A clue to this issue is the proximity to collinear spin phases, i.e. the A-type and E-type spin phases. Near the phase boundary, the spin configuration is not a simple spiral but is subject to the significant elliptical modulation and contains higher harmonics [17], which is sensitively enhanced by the tiny spin-phonon coupling or by

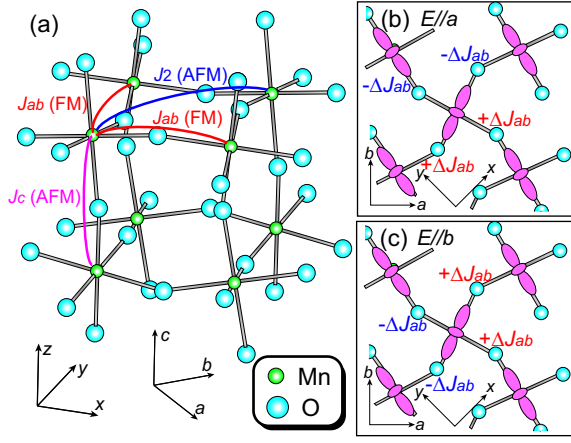


FIG. 1: (Color online) (a) Superexchange interactions in  $RMnO_3$  described by the Hamiltonian Eq. (2). (b) Modulations of the in-plane nearest-neighbor ferromagnetic exchanges under  $\mathbf{E}||a$ . (c) Those under  $\mathbf{E}||b$ . Here FM and AFM denote ferromagnetic and antiferromagnetic exchanges, respectively.

the weak magnetic anisotropy. In this paper, we study the role of this higher harmonics on the electromagnon excitation, and resolve the long standing puzzle of the OS in the terahertz-frequency regime.

We start with a realistic spin model for the Mn perovskites [7]. The model is basically a classical Heisenberg model on a cubic lattice, which contains the frustrating spin exchanges, the DM interaction, the single-ion spin anisotropies, and the biquadratic interaction. The Mn spins are treated as classical vectors. The Hamiltonian consists of five terms as  $\mathcal{H} = \mathcal{H}_{\text{ex}} + \mathcal{H}_{\text{sia}}^D + \mathcal{H}_{\text{sia}}^E + \mathcal{H}_{\text{DM}} + \mathcal{H}_{\text{biq}}$ , with

$$\mathcal{H}_{\text{ex}} = \sum_{\langle i,j \rangle} J_{ij} \mathbf{S}_i \cdot \mathbf{S}_j, \quad (2)$$

$$\mathcal{H}_{\text{sia}}^D = D \sum_i S_{\zeta i}^2, \quad (3)$$

$$\mathcal{H}_{\text{sia}}^E = E \sum_i (-1)^{i_x+i_y} (S_{\xi i}^2 - S_{\eta i}^2), \quad (4)$$

$$\mathcal{H}_{\text{DM}} = \sum_{\langle i,j \rangle} \mathbf{d}_{ij} \cdot (\mathbf{S}_i \times \mathbf{S}_j), \quad (5)$$

$$\mathcal{H}_{\text{biq}} = -B_{\text{biq}} \sum_{\langle i,j \rangle} (\mathbf{S}_i \cdot \mathbf{S}_j)^2, \quad (6)$$

where  $i_x$ ,  $i_y$  and  $i_z$  represent coordinates of the  $i$ -th Mn ion with respect to the cubic  $x$ ,  $y$  and  $z$  axes. For the  $a$ ,  $b$  and  $c$  axes, we adopt the  $P_{bnm}$  notation [see Fig. 1(a)]. The first term  $\mathcal{H}_{\text{ex}}$  describes the superexchange interactions as shown in Fig. 1(a). The frustration between ferromagnetic  $J_{ab}$  and antiferromagnetic  $J_2$  in the  $ab$  plane results in a spiral spin order, while the inter-plane antiferromagnetic  $J_c$  causes a staggered stacking along the  $c$  axis. The terms  $\mathcal{H}_{\text{sia}}^D$  and  $\mathcal{H}_{\text{sia}}^E$  stand for the single-ion

anisotropies.  $\mathcal{H}_{\text{sia}}^D$  makes the magnetization along the  $c$  axis hard. On the other hand,  $\mathcal{H}_{\text{sia}}^E$  causes an alternate arrangement of the local hard and easy magnetization axes in the  $ab$  plane due to the staggered orbitals. The term  $\mathcal{H}_{\text{DM}}$  denotes the DM interaction. The DM vectors  $\mathbf{d}_{ij}$  associated with Mn-O-Mn bonds are expressed using five DM parameters as given in Ref. [18] because of the crystal symmetry;  $\alpha_{ab}$ ,  $\beta_{ab}$  and  $\gamma_{ab}$  for  $\mathbf{d}_{ij}$  on the in-plane bonds, while  $\alpha_c$  and  $\beta_c$  for  $\mathbf{d}_{ij}$  on the inter-plane bonds. The last term  $\mathcal{H}_{\text{biq}}$  represents the biquadratic interaction working between adjacent two spins in the  $ab$ -plane, which originates from the spin-phonon coupling [19]. We have microscopically determined the parameter values [7].

We perform calculations using two sets of the model parameters (A and B) as (A)  $J_{ab}=-0.74$ ,  $J_2=0.74$ ,  $J_c=1.2$ ,  $(\alpha_{ab}, \beta_{ab}, \gamma_{ab})=(0.1, 0.1, 0.16)$ ,  $(\alpha_c, \beta_c)=(0.4, 0.1)$ ,  $D=0.24$ ,  $E=0.3$ , and  $B_{\text{biq}}=0.025$ , and (B)  $J_{ab}=-0.7$ ,  $J_2=0.96$ ,  $J_c=1.0$ ,  $(\alpha_{ab}, \beta_{ab}, \gamma_{ab})=(0.1, 0.1, 0.12)$ ,  $(\alpha_c, \beta_c)=(0.45, 0.1)$ ,  $D=0.2$ ,  $E=0.25$ , and  $B_{\text{biq}}=0.025$ . Here the energy unit is meV. These parameter sets give the  $ab$ -plane spin spiral propagating along the  $b$  axis with six times periodicity ( $q_b=\pi/3$ ) and the  $bc$ -plane one with five times periodicity ( $q_b=2\pi/5$ ), respectively. The former spin state resembles the  $ab$ -plane spiral in  $\text{Eu}_{1-x}\text{Y}_x\text{MnO}_3$  ( $x=0.45$ ) with  $q_b \sim 0.3\pi$ , while the latter resembles the  $bc$ -plane spiral in  $\text{DyMnO}_3$  with  $q_b=0.39\pi$ . Note that we adopt the commensurate spin states for convenience of the finite-size calculations, whereas the actual spin states are incommensurate. However, conclusions of this paper are never affected by this difference. Sizes of the systems used are  $20 \times 20 \times 6$  and  $18 \times 18 \times 6$  for respective cases, which match the periodicities of spirals.

We study the electromagnon and magnon excitations by numerically solving the Landau-Lifshitz-Gilbert equation using the fourth-order Runge-Kutta method. The equation is given by

$$\frac{\partial \mathbf{S}_i}{\partial t} = -\mathbf{S}_i \times \mathbf{H}_i^{\text{eff}} + \frac{\alpha_G}{S} \mathbf{S}_i \times \frac{\partial \mathbf{S}_i}{\partial t}, \quad (7)$$

where  $\alpha_G (=0.1-0.2)$  is the dimensionless Gilbert-damping coefficient. We derive an effective local magnetic field  $\mathbf{H}_i^{\text{eff}}$  acting on the  $i$ -th Mn spin  $\mathbf{S}_i$  from the Hamiltonian  $\mathcal{H}$  as  $\mathbf{H}_i^{\text{eff}} = -\partial \mathcal{H} / \partial \mathbf{S}_i$ . Considering the strong reduction of the Mn magnetic moment revealed by neutron-scattering experiment [17], we set  $|\mathbf{S}|=1.4$ .

For the origin of the electromagnon excitation, we consider the coupling  $-\mathbf{E} \cdot \mathbf{P}$  between the external electric field  $\mathbf{E}$  and the spin-dependent electric polarizations  $\mathbf{P}$  given by Eq. (1). Noticeably this coupling effectively modulates the nearest-neighbor ferromagnetic exchanges in the  $ab$  plane from  $J_{ab} \mathbf{S}_i \cdot \mathbf{S}_j$  to  $(J_{ab} + \mathbf{E} \cdot \boldsymbol{\Pi}_{ij}) \mathbf{S}_i \cdot \mathbf{S}_j$ . More concretely, the application of  $\mathbf{E}||a$  [ $\mathbf{E}||b$ ] corresponds to modulations of the in-plane spin exchanges shown in Fig. 1(b) [Fig. 1(c)].

We apply the electric field  $\mathbf{E}||a$  or  $\mathbf{E}||b$  as a short pulse

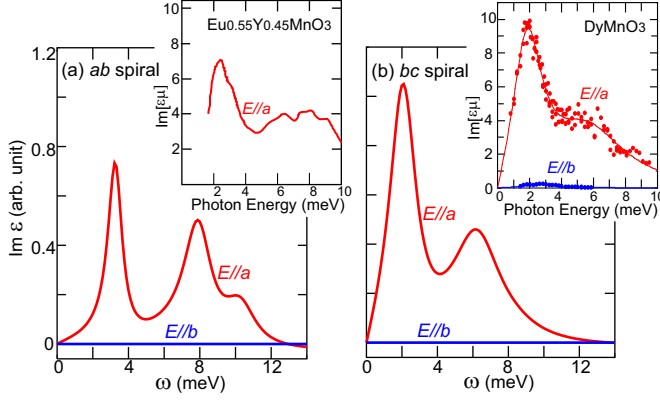


FIG. 2: (Color online) Calculated electromagnon optical spectra for (a) *ab*-plane spiral state ( $q_b = \pi/3$ ) with parameter set A, and (b) *bc*-plane spiral state ( $q_b = 2\pi/5$ ) with parameter set B. Values of  $\alpha_G$  used for the calculations are 0.1 and 0.2 for (a) and (b), respectively. Insets show the experimental spectra of  $\text{Eu}_{0.55}\text{Y}_{0.45}\text{MnO}_3$  [16] and  $\text{DyMnO}_3$  [11], respectively.

at  $t=0$ . Then we trace the time evolution of  $\mathbf{P}$  given by Eq. (1). The electromagnon spectrum,  $\text{Im } \epsilon(\omega)$ , is calculated from the Fourier transformation of  $\mathbf{P}(t)$ .

In Fig. 2, we depict calculated electromagnon spectra for the cases of (a) *bc*-plane spiral state with parameter set A and (b) *ab*-plane spiral state with parameter set B. Irrespective of the spiral-plane orientation, large spectral weight emerges at low energy when  $\mathbf{E} \parallel \mathbf{a}$ . In contrast, we observe no response to  $\mathbf{E} \parallel \mathbf{b}$  for both cases in agreement with the experiment [12]. For comparison, we display the experimental spectrum of  $\text{Eu}_{0.55}\text{Y}_{0.45}\text{MnO}_3$  [16] and that of  $\text{DyMnO}_3$  [11] in the insets. For both cases, we obtain fairly good agreement between theory and experiment. In the following, we discuss the results for the *ab*-plane spiral case. Similar discussion can be repeated for the *bc*-plane spiral case.

To identify origin of the two-peak structure of the electromagnon spectrum, we calculate electromagnon spectra and magnon-dispersion spectra along  $\mathbf{k} = (0, k_b, 0)$ , for various cases of interactions (see Fig. 3). The magnon spectra are calculated from the Fourier transformation of the space- and time-domain simulation data for the spin dynamics of  $\delta S \parallel (\textit{ab}\text{-spiral plane})$  after applying  $H$  as a short pulse to a single-site spin in the *ab*-spiral ground state. When the Hamiltonian consists of only the spin-exchange term and the single-ion anisotropy  $D$  term, i.e.,  $\mathcal{H}_{\text{ex}}$  and  $\mathcal{H}_{\text{sia}}^D$  [see Fig. 3(a)], the spin spiral has a uniform rotation angle. In practice, for the case of pure spiral order, translational symmetry is conserved upon the one lattice-unit translation if it is accompanied by an appropriate rotation of the spin axes. Then despite the long-period magnetic structure, matrix elements which mix magnon branches do not exist. In this case, we can see only one peak at a rather high energy of  $\sim 8$  meV corresponding to that in Fig. 3(a). Incorporation of the

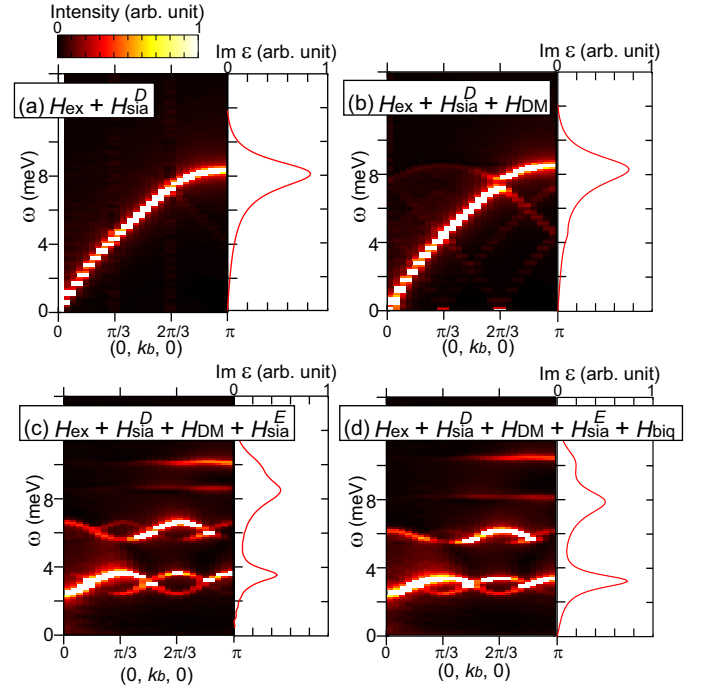


FIG. 3: (Color online) Calculated intensity map of magnon (left panel) and electromagnon OS (right panel) for each Hamiltonian with successively adding the interactions. (a)  $\mathcal{H}_{\text{ex}} + \mathcal{H}_{\text{sia}}^D$  giving a spin spiral with a uniform rotation angle. (b) Adding  $\mathcal{H}_{\text{DM}}$  induces negligibly small changes. (c) Incorporation of  $\mathcal{H}_{\text{sia}}^E$  causes the elliptical deformation or higher harmonics of the spin spiral, resulting in the magnon foldings and evolution of the lower-energy peak in the OS. (d) For full Hamiltonian including also  $\mathcal{H}_{\text{biq}}$ , the lower-energy peak in the OS is further enhanced.

DM interaction  $\mathcal{H}_{\text{DM}}$  does not change the spectral shape [see Fig. 3(b)].

Further adding the single-ion anisotropy  $E$  term  $\mathcal{H}_{\text{sia}}^E$  gives rise to folding and anticrossing of the magnon dispersions. Namely, in the extended Brillouin zone picture, magnon branches separated by the reciprocal lattice vector  $\mathbf{G} = (0, q_b, 0)$  are mixed with each other where  $q_b = \pi/3$  in the present case. This gives rise to changes in the spectral shape, i.e. another peak of the OS at a lower energy of  $\sim 3$  meV appears, and the higher-lying peak slightly splits into two peaks as shown in Fig. 3(c). Finally we can see dramatic enhancement of the lower-lying peak in the OS when the Hamiltonian is full including the bi-quadratic term  $\mathcal{H}_{\text{biq}}$  as shown in Fig. 3(d). Comparing the electromagnon spectra with the magnon spectra at the zone edge, i.e.  $\mathbf{k} = (0, \pi, 0)$ , we indeed confirm that the electromagnon corresponds to the magnon modes hybridized with the zone-edge state due to the form factor of the magnetoelectric coupling in Eq. (1) as described in Ref. [13]. Strong magnon anticrossing causes rather flat magnon dispersions. The magnon branches predicted here would be observed experimentally.

We can see vital roles of the single-ion anisotropy  $\mathcal{H}_{\text{sia}}^E$

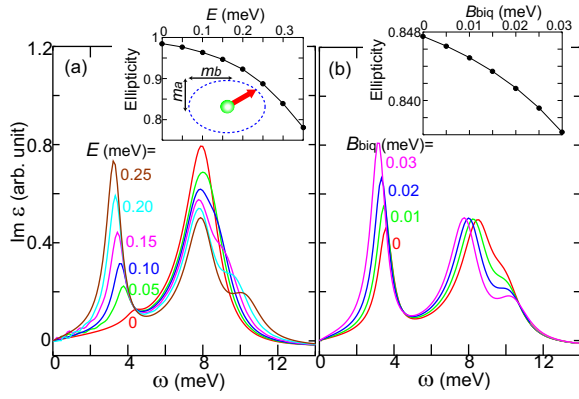


FIG. 4: (Color online) Calculated electromagnon spectra for various strength of (a) single-ion anisotropy  $E$  and (b) biquadratic interaction  $B_{\text{biq}}$ . Insets show calculated ellipticity of the  $ab$ -plane spin spiral ( $m_a/m_b$ ) as functions of  $E$  and  $B_{\text{biq}}$ , respectively.

and the biquadratic interaction  $\mathcal{H}_{\text{biq}}$  in Figs. 4(a) and 4(b), which show the calculated spectra for various values of the coupling constants  $E$  and  $B_{\text{biq}}$ , respectively. Surprisingly the lower-lying peak is enhanced strongly by the weak anisotropy or by the tiny biquadratic interaction. In the insets of Figs. 3(a) and 3(b), we show calculated ellipticity of the spin spiral for each case, which is defined as the ratio of amplitudes between the  $a$ -axis spin component and the  $b$ -axis spin component ( $m_a/m_b$ ) [20]. We see that the enhancement of the low-lying peak are accompanied by the decrease of ellipticity. Note that the elliptical deformation of the spin spiral is more significant when the ellipticity is decreased more from unity. This indicates that the origin of the low-energy peak at  $\sim 2$ -3 meV is the magnon-branch mixing due to the elliptical modulation of the spin spiral.

Let us now discuss the  $R$  dependence of the electromagnon spectra of  $\text{RMnO}_3$ . In  $\text{TbMnO}_3$ , the spectrum has more weight at the higher-energy peak [15], while in  $\text{DyMnO}_3$  with a smaller ionic  $R$ -site radius ( $r_R$ ), the spectral weight is shifted to lower energy [11]. In the systematic study of  $\text{Eu}_{1-x}\text{Y}_x\text{MnO}_3$ , transfer of the spectral weight to lower energies has been reported as the  $Y$  content  $x$  is increased (or as the averaged  $r_R$  is decreased) [15]. Note that with decreasing  $r_R$ , we approach the E-type phase, which results in a stronger influence of the biquadratic interaction. So far, the magnon spectrum in  $\text{RMnO}_3$  with a spiral spin order has only been reported for  $\text{TbMnO}_3$  [21]. In the compounds closer to the E-type phase, we expect that the magnon spectrum exhibits significant foldings. Further experimental data for these compounds are necessary to examine our theory.

In some of the  $\text{RMnO}_3$  compounds, deviation of frequencies between the magnetic resonance and the electromagnon has been reported [22]. Within our theory, the frequency of the magnetic resonance at the zone center

$\mathbf{k}=0$  coincides with that of the electromagnon at  $\mathbf{k}=(0, \pi, 0)$  only if they are connected with a multiple of  $\mathbf{G}=(0, q_b, 0)$ . When the spiral magnetic order is incommensurate, magnetic resonance and electromagnon absorption occur at different points in the Brillouin zone. Thus frequencies of these two spectra do not necessarily coincide with each other.

In summary, we have studied the electromagnon dynamics taking into account all the relevant interactions and anisotropies in the spin Hamiltonian for  $\text{RMnO}_3$ . It is found that the elliptical modulation or higher harmonics of the ground-state spiral spin configuration has crucial influences on the foldings of the magnon dispersion and also the electromagnon spectrum, which resolves the long standing puzzle of the low energy peak in the OS.

The authors are grateful to N. Kida, S. Miyahara, Y. Takahashi, J. S. Lee, and Y. Tokura for fruitful discussions. This work was supported in part by Grant-in-Aids (Grant No.19048015, No.19048008, No.21244053 and No.17105002) and NAREGI Nanoscience Project from the Ministry of Education, Culture, Sports, Science, and Technology.

\* Electronic address: mochizuki@erato-mf.t.u-tokyo.ac.jp

† Electronic address: furukawa@phys.aoyama.ac.jp

‡ Electronic address: nagaosa@appi.t.u-tokyo.ac.jp

- [1] For recent reviews on the multiferroics, see M. Fiebig, J. Phys. D: Appl. Phys. **38**, R123 (2005); Y. Tokura, Science **312**, 1481 (2006); W. Eerenstein, N. D. Mathur, and J. F. Scott, Nature (London) **442**, 759 (2006); S.-W. Cheong and M. Mostovoy, Nat. Mater. **6**, 13 (2007); Y. Tokura, J. Magn. Magn. Mater. **310**, 1145 (2007); D. I. Khomskii, J. Magn. Magn. Mater. **306**, 1 (2006).
- [2] T. Kimura, T. Goto, H. Shintani, K. Ishizaka, T. Arima, and Y. Tokura, Nature (London) **426**, 55 (2003).
- [3] H. Katsura, N. Nagaosa, and A. V. Balatsky, Phys. Rev. Lett. **95**, 057205 (2005).
- [4] M. Mostovoy, Phys. Rev. Lett. **96**, 067601 (2006).
- [5] I. A. Sergienko and E. Dagotto, Phys. Rev. B **73**, 094434 (2006).
- [6] G. A. Smolenski and I. E. Chupis, Usp. Fiziol. Nauk **137**, 415 (1982) [Sov. Phys. Usp. **25**, 475 (1982)].
- [7] M. Mochizuki, and N. Furukawa, J. Phys. Soc. Jpn. **78**, 053704 (2009); Phys. Rev. B **80**, 134416 (2009).
- [8] A. Pimenov, A. A. Mukhin, V. Yu. Ivanov, V. D. Travkin, A. M. Balbashov, and A. Loidl, Nat. Phys. **2**, 97 (2006).
- [9] A. Pimenov, T. Rudolf, F. Mayr, A. Loidl, A. A. Mukhin, and A. M. Balbashov, Phys. Rev. B **74**, 100403(R) (2006).
- [10] H. Katsura, A. V. Balatsky, and N. Nagaosa, Phys. Rev. Lett. **98**, 027203 (2007).
- [11] N. Kida, Y. Ikebe, Y. Takahashi, J. P. He, Y. Kaneko, Y. Yamasaki, R. Shimano, T. Arima, N. Nagaosa, and Y. Tokura, Phys. Rev. B **78**, 104414 (2008).
- [12] N. Kida, Y. Yamasaki, R. Shimano, T. Arima, and Y. Tokura, J. Phys. Soc. Jpn. **77**, 123704 (2008).
- [13] R. ValdesAguilar, M. Mostovoy, A. B. Sushkov, C. L.

- Zhang, Y. J. Choi, S-W. Cheong, and H. D. Drew, Phys. Rev. Lett. **102**, 047203 (2009).
- [14] S. Miyahara and N. Furukawa, arXiv:0811.4082.
  - [15] Y. Takahashi, N. Kida, Y. Yamasaki, J. Fujioka, T. Arima, R. Shimano, S. Miyahara, M. Mochizuki, N. Furukawa, and Y. Tokura, Phys. Rev. Lett. **101**, 187201 (2008).
  - [16] Y. Takahashi, Y. Yamasaki, N. Kida, Y. Kaneko, T. Arima, R. Shimano, and Y. Tokura, Phys. Rev. B **79**, 214431 (2009).
  - [17] T. Arima, A. Tokunaga, T. Goto, H. Kimura, Y. Noda, and Y. Tokura, Phys. Rev. Lett. **96**, 097202 (2006).
  - [18] I. Solov'yev, N. Hamada, and K. Terakura, Phys. Rev. Lett. **76**, 4825 (1996).
  - [19] T. A. Kaplan, Phys. Rev. B **80**, 012407 (2009).
  - [20] Y. Yamasaki, H. Sagayama, T. Goto, M. Matsuura, K. Hirota, T. Arima, and Y. Tokura, Phys. Rev. Lett. **98**, 147204 (2007).
  - [21] D. Senff, P. Link, K. Hradil, A. Hiess, L. P. Regnault, Y. Sidis, N. Aliouane, D. N. Argyriou, and M. Braden, Phys. Rev. Lett. **98**, 137206 (2007).
  - [22] N. Kida, Y. Takahashi, J. S. Lee, R. Shimano, Y. Yamasaki, Y. Kaneko, S. Miyahara, N. Furukawa, T. Arima, and Y. Tokura, J. Opt. Soc. Am. B **26**, A35 (2009).